ANL/MSD/PP--80487

A UNIFIED DESCRIPTION OF CRYSTALINE-TO-AMORPHOUS TRANSITIONS*

N. Q. LAM[1], P. R. OKAMOTO[1], R DEVANATHAN[1,2] and M. MESHII[2]

[1]Materials Science Division, Argonne National Laboratory, Argonne, IL 60439,

2Department of Materials Science and Engineering, Northwestern University, Evanston, IL 60208

July 1993

DISCLAIMER

*Work supported by the U.S. Department of Energy, BES-Materials Sciences, under Contract W-31-109-Eng-38, and by the National Science Foundation, under Grant DMR 8802847.

A UNIFIED DESCRIPTION OF CRYSTALLINE-TO-AMORPHOUS TRANSITIONS

N. Q. LAM[1], P. R. OKAMOTO[1], R. DEVANATHAN[1,2] and M. MESHII[2]

[1] Materials Science Division, Argonne National Laboratory, Argonne, IL 60439

[2] Department of Materials Science and Engineering, Northwestern University, Evanston, IL 60208

ABSTRACT

The fact that amorphous metallic alloys can now be synthesized by a variety of solid-state processes underscores the need for a more general approach to crystalline-to-amorphous (c-a) transitions. By focusing on static atomic displacements as a generic measure of chemical and topological disorder, we show that a unified description of c-a transformations can be based on a generalization of the phenomenological melting criterion proposed by Lindemann. The generalized version assumes that melting of a defective crystal occurs whenever the sum of thermal and static mean-square displacements exceeds a critical value identical to that for melting of the defect-free crystal. This assumption implies that chemical or topological disorder measured by static displacements is thermodynamically equivalent to heating, and therefore that the melting temperature of the defective crystal will decrease with increasing amount of disorder. This in turn implies the existence of a critical state of disorder where the melting temperature becomes equal to a glass-transition temperature below which the metastable crystal melts to a glass. The generalized Lindemann melting criterion thus leads naturally to an interpretation of c-a transformations as defect-induced, low-temperature melting of critically disordered crystals. Direct confirmation of this criterion is provided by molecular-dynamics simulations of heat-induced melting and of defect-induced amorphization of intermetallic compounds caused either by the production of Frenkel pairs or anti-site defects. The thermodynamic equivalence between static atomic disorder and heating is reflected in the identical softening effects which they have on elastic properties and also in the diffraction analysis of diffuse scattering from disordered crystals, where the effect of static

displacements appears as an artificially-enlarged thermal Debye-Waller factor. Predictions of this new, unified approach to melting and amorphization are compared with available experimental information.

PACS: 61.50.Ks, 64.60.My, 81.30.Hd

1. INTRODUCTION

Several solid-state amorphizing processes were discovered during the past two decades.[1] Crystalline-to-amorphous (c-a) transitions can now be induced by particle irradiation (including ion beam mixing and ion implantation), mechanical alloying, interdiffusion reactions during thermal annealing of bimetallic multilayered thin films, hydrogen charging, and in some cases by subjecting the materials to high pressures. Extensive investigations of the various fundamental aspects of amorphization have been carried out in recent years, and fresh insights into the phenomenon have been obtained.

The majority of the basic studies concentrated on radiation-induced amorphization. In fact, the possibility of amorphizing ordered compounds by MeV electrons inside a high-voltage electron microscope, first demonstrated by Carpenter and Schulson[2] and extensively investigated by Mori et al.,[3] has stimulated numerous systematic experiments, because electron irradiation has been recognized as the simplest and the most controllable way of destabilizing a crystalline lattice. On the theoretical side, the simple nature of electron damage has also motivated several molecular dynamics simulations of amorphizing transformations, since only Frenkel pairs and anti-site defects are involved and, hence, concepts like thermal spike and local quenching can be neglected. The knowledge attained from these studies has been essential for the development of a general description of solid-state amorphization.

Investigations on various ordered intermetallics have revealed that amorphizable materials have a number of common features.[4] For example, during irradiation, the Bragg-Williams long-range order parameter S decreases rapidly from 1 (i.e., the value for the perfect lattice) to below ~0.5,[5-8] and the volume of the compound expands with increasing dose. *In situ* electron diffraction and Brillouin scattering studies of intermetallic compounds revealed a correlation between the onset of amorphization and a critical volume expansion (a few percents[7,9]) of the parent phase. This isothermal-isobaric expansion associated with chemical disordering and Frenkel-pair production was found to cause dramatic elastic softening. Measurements in ion-bombarded FeTi, Nb_3Ir, and Zr_3Al, all of which can be amorphized readily under selected

experimental conditions, showed large decreases (~50%) in the shear modulus during disordering, whereas only small decreases (≤15%) were found for NiAl and FeAl, which do not amorphize under the same conditions.[4] TEM investigations revealed that the elastic softening also manifests itself in quasi-periodic striations in bright-field images and pronounced streaking in diffraction patterns,[6,9] both of which indicate that $C' = 0.5(C_{11} - C_{12})$ softens substantially more than C_{44}. These results demonstrated that elastic instability is a characteristic feature of solid-state amorphization. Recent work has also brought forth evidence indicating the existence of parallels between melting and amorphization.[4] A fundamental study of these thermodynamic parallels will thus not only provide the basis for understanding solid-state amorphizing transformations in general, but will also lead to new insights into the melting process.

In the present paper, a new approach to an understanding of these features and similarities is proposed. From a diffraction point of view, static atomic displacements in crystalline materials can often be characterized in terms of an artificially-enlarged thermal Debye-Waller factor in which the thermal and static mean-square atomic displacements appear additively. By assuming that this equivalence between thermal and static displacements extends beyond diffraction effects per se, a unified thermodynamic description of solid-state amorphization can be formulated within the framework of a generalized Lindemann melting criterion. This approach also leads to a thermo-elastic criterion for predicting the relative susceptibility of different compounds to amorphization. It will be shown that this unified description is well supported by both the results of our molecular dynamics simulations and recent experimental observations of irradiation-induced amorphization.

2. SOLID-STATE AMORPHIZATION AS A DISORDER-INDUCED MELTING PROCESS

2.1. Generalized Lindemann Melting Criterion for Amorphization

The original Lindemann criterion[10] proposed that an ideal crystal melts when the root-mean-square amplitude of thermal vibrations, $\langle\mu^2_{vib}\rangle^{1/2}$, exceeds a critical value $\langle\mu^2_{cri}\rangle^{1/2}$,

which is some critical fraction of the nearest-neighbor distance. The mechanical melting temperature T_m of the crystal is related to $<\mu_{cri}^2>$ by[11]

$$T_m = \frac{Mk\theta_c^2}{9\hbar^2} <\mu_{cri}^2> \qquad (1)$$

where M is the atomic mass, k the Boltzmann constant, and θ_c the Debye temperature of the *perfect* crystal.

In the case of defective crystals, lattice imperfections such as chemical disorder and Frenkel pairs can give rise to an additional static component, $<\mu_{sta}^2>$, to the mean-square atomic displacement. Hence, as suggested by Voronel et al.,[12] the Lindemann criterion should be applied to the total mean square displacement $<\mu_T^2>$, which, by assuming statistical independence, is the sum of $<\mu_{vib}^2>$ and $<\mu_{sta}^2>$:

$$<\mu_T^2> = <\mu_{vib}^2> + <\mu_{sta}^2> \qquad (2)$$

That is, a defective crystal becomes destabilized whenever $<\mu_T^2>$ exceeds $<\mu_{cri}^2>$, i.e., at a temperature T_d given by

$$T_d = \frac{Mk\theta_d^2}{9\hbar^2} <\mu_{cri}^2>, \qquad (3)$$

where θ_d, the Debye temperature of the *defective* crystal, is scaled with θ_c in the form

$$\theta_d^2 = \theta_c^2\left[1 - \frac{<\mu_T^2>}{<\mu_{cri}^2>}\right] \quad . \qquad (4)$$

Here, it is the total magnitude of atomic displacements that is of critical importance, not the details of the displacement-producing process. By treating the dominant static component of atomic displacements as frozen heat motion, the original form of the linear Lindemann relationship between the melting temperature and the square of the Debye temperature is recovered. However, as shown by eq. (4), the Debye temperature and, hence, the 'melting' temperature at constant

pressure of the defective crystal are no longer constant; they decrease linearly with increasing state of disorder as measured by $<\mu_T^2>$.

Equations (1), (3) and (4) lead to the following scaling relationships

$$\frac{T_d}{T_m}=\frac{\theta_d^2}{\theta_c^2}=\frac{G_d}{G_c}=1-\frac{<\mu_T^2>}{<\mu_{cri}^2>} \tag{5}$$

with G_c and G_d being the average shear elastic constants of the perfect and defective crystals, respectively. Thus,

for $<\mu_T^2>=0$, $\theta_d=\theta_c$, $G_d=G_c$ and $T_d=T_m$ (6)

and as $<\mu_T^2> \rightarrow <\mu_{cri}^2>$, $\theta_d \rightarrow 0$, $G_d \rightarrow 0$ and $T_d \rightarrow 0$ (7)

Equation (7) represents the condition for *mechanical* melting. However, as discussed in the following section, amorphization can take place via a first-order transition before $<\mu_T^2>$ reaches $<\mu_{cri}^2>$. This can occur when $<\mu_T^2>$ equals $<\mu_{cri}^2>^t$, which corresponds to a critical state of disorder analogous to that of *thermodynamic* melting (Fig. 1), where the enthalpy of the defective crystal becomes equal to that of the glassy state.

2.2. Thermo-elastic Criterion for Amorphization

Amorphization becomes thermodynamically possible whenever the total increase in enthalpy caused by lattice imperfections exceeds the enthalpy of crystallization, i.e., the enthalpy difference between the amorphous and crystalline states. Application of the generalized Lindemann criterion to both the crystalline solid and its glassy state shows that the enthalpy difference between the two phases is directly related to the difference in their Debye temperatures. Relative to the defect-free crystal, the enthalpy of crystallization can be written as[4]

$$\Delta H_c = L_c\left[1-\frac{\theta_a^2}{\theta_c^2}\right], \tag{8}$$

where L_c is the pertinent heat of fusion and the subscript 'a' denotes the amorphous state. This relation is consistent with the free-energy change for a polymorphous phase transformation, which includes Debye temperatures and electronic specific heat contributions.[13]

The crystallization enthalpy of the defective crystal, ΔH_d, can also be expressed in the same form as eq. (8) with the subscript 'c' replaced by 'd', so that it scales with ΔH_c according to

$$\Delta H_d = \Delta H_c \left[\frac{\theta_d^2 - \theta_a^2}{\theta_c^2 - \theta_a^2} \right]. \qquad (9)$$

Thus, ΔH_d will vanish whenever the defective crystal is driven to a critical state of disorder where its Debye temperature becomes equal to that of the amorphous phase. As shown schematically in Fig. 1, this condition can be used to define a critical temperature T_a in the sense that a thermodynamic driving force for amorphization exists below this temperature where ΔH_d is negative, but not at higher temperatures. Application of the Lindemann criterion to the glassy state implies that T_a is the melting temperature of the glass and, hence, can be interpreted as the glass transition temperature. Moreover, when combined with eq. (5), eq. (9) shows that

$$\text{as} \quad \langle \mu_T^2 \rangle \rightarrow \langle \mu_{cri}^2 \rangle^t \;, \quad \theta_d \rightarrow \theta_a \;, \quad G_d \rightarrow G_a \;, \quad \Delta H_d \rightarrow 0 \;, \quad \text{and} \quad T_d \rightarrow T_a . \qquad (10)$$

Thus, eq. (10) can be considered as the necessary condition for *thermodynamic* melting of a defective crystal to a glass. However, if the transition is kinetically suppressed for $\Delta H_d << 0$, the 'superheated' defective crystal can be driven to a critical state of disorder where $\langle \mu_T^2 \rangle = \langle \mu_{cri}^2 \rangle^m$, and therefore $G_d = 0$, i.e., *mechanical* melting may occur.

2.3. Results of Molecular Dynamics Simulations

Several fundamental aspects of solid-state amorphizing transformations were elucidated by molecular-dynamics simulations of radiation-induced amorphization. Here, we monitored (i) the thermodynamic response of ordered compounds during chemical disordering and generation of Frenkel pairs, including increases in the system volume and potential energy and mean-square

atomic displacements; (ii) changes in the compound microstructure, characterized by pair-correlation functions, structure factors, atomic projections and single-crystal diffraction patterns; and (iii) changes in the mechanical properties, i.e., the irradiation-dose dependence of the shear elastic constants. Eight intermetallic compounds have been simulated: four compounds of the Cu-Ti system,[14-16] two compounds of the Ni-Zr system,[17,18] NiTi,[19] and FeTi. The simulational procedure[14,15,17] and appropriate embedded-atom potentials[14,17] that governed the interactions between atoms in these intermetallics have been described elsewhere. Several important observations have been made:

A. In order for a compound to become amorphous, the necessary (but not sufficient) condition is that its potential energy and volume must be increased to the corresponding levels of the quenched liquid.

We can classify the compounds under study into three groups: (i) The compounds NiZr and $NiZr_2$ can be amorphized easily, either by chemical disordering or by introduction of Frenkel pairs.[17,18] As an example, Fig. 2 shows changes in the potential energy, volume and microstructure of NiZr with increasing damage dose in dpa (displacements or Frenkel pairs per atom) or epa (exchanges per atom). The evolution of the microstructure is indicated by progressive changes in the calculated pair-correlation function g(r), diffraction pattern and lattice image. At the point when the thermodynamic propeties of the defective compound become equal to those of the quenched NiZr liquid (i.e., at ~0.2 dpa or epa), g(r) and lattice images show amorphous features, the superlattice spots disappear and diffuse halos appear on the diffraction patterns. In an earlier molecular-dynamics simulation with tight-binding potentials, Massobrio et al.[20] have also shown that chemical disorder led to amorphization of $NiZr_2$. (ii) The compounds Cu_4Ti_3, CuTi, $CuTi_2$, and FeTi can be amorphized only by the introduction of Frenkel pairs. The same tendency was also found for NiTi; however, this result is taken with some caution because the interaction potential used for this compound was fitted to the less-stable B2 structure.[19] (iii) Cu_4Ti could not be rendered amorphous, either by antisite defects nor Frenkel pairs, which is entirely consistent with experiments showing that among all the equilibrium compounds of the Cu-Ti alloy system,

only Cu_4Ti remains crystalline under electron irradiation.[21] Our simulations indicated, however, that this compound might be amorphized by ion bombardment.[15]

B. In compounds that are amorphizable, the shear elastic constants C_{44} and $C' \equiv 0.5(C_{11} - C_{12})$ first decrease rapidly with increasing dose, and then, near the onset of amorphization, C' turns around, increasing toward the value of C_{44}.[15-18] The shear constants C_{44} and C' become equal to each other when amorphization has been completed, i.e., the system becomes elastically isotropic. As a result, the average shear modulus $G_d = 0.5(C_{44} + C')$ drops monotonically in the early stage of irradiation and attains to a constant value after the onset of amorphization.

C. The average shear modulus G_d of the defective compound decreases much faster with the isothermal volume expansion caused by defect production than the thermal expansion of the perfect crystal, G_c, during heating. Both these moduli attained the same critical value when amorphization and melting occured, respectively. This value is approximately half of that calculated for the perfect crystal near 0 K. Examples are illustrated in Figs. 3A and 4A for NiZr and $NiZr_2$. The large decrease in the shear constants found at the onset of amorphization is in good agreement with the elastic softening observed experimentally in the three compounds FeTi, Nb_3Ir and Zr_3Al during Kr^+ bombardment[4] and with the results of earlier silmulations.[22,23] In addition, significant differences between the shear moduli of the crystalline and amorphous materials were measured[24-29] and estimated from theoretical considerations.[30-32]

The faster drop of G_d with volume expansion due to defect introduction, relative to that for thermal expansion of the defect-free crystal, appears at first to contradict earlier computer simulations of melting in Cu[33] which showed that the volume dependence of the shear constants C_{44} and C' during homogeneous expansion at constant temperature was virtually identical to that associated with thermal expansion at constant pressure. This implied that the volume dependence of the elastic constant did not depend on how the expansion was produced. However, it is now recognized that this remarkable behavior is a consequence of the uniform nature of the volume expansions employed in the earlier simulations. In contrast to uniform thermal expansion which

does not involve changes in chemical long-range order, the volume expansion associated with chemical disordering and/or Frenkel pairs is brought about by static atomic displacements. It was found that the increase in $\Delta V/V$ per unit mean-square displacement was significantly larger for thermal displacements than with static displacements (Figs. 3B and 4B).

D. As a consequence, although the volume expansions required for melting and amorphization were drastically different, the decrease in the average shear modulus with increasing $\langle\mu_T^2\rangle$ was found to be the same for both melting and amorphization processes (Figs. 3C and 4C), consistent with the prediction of eqs. (4)-(5).

Although $\langle\mu_T^2\rangle$ is an average quantity that is experimentally measurable, its calculation is not straightforward in the case of Frenkel pairs where large artificial displacements are introduced. However, a true measure of $\langle\mu_T^2\rangle$ can be obtained from the mean-square dispersion in the average nearest-neighbor distance, $\langle\sigma^2\rangle$,[18] which, as shown in Fig. 5 for the heating case, is directly proportional to $\langle\mu_T^2\rangle$. The same linear relationship between $\langle\sigma^2\rangle$ and $\langle\mu_T^2\rangle$ was also demonstrated previously by Sevillano et al. for pure metals.[34] As a result, when plotted as a function of $\langle\sigma^2\rangle$, the values of G_d for isobaric melting and for amorphization induced by anti-site defects or Frenkel pairs lie on the same curve (Figs. 3D and 4D). It can be seen that once the compound has been amorphized, both G_d and $\langle\sigma^2\rangle$ no longer change ($\equiv G_a$ and $\langle\sigma_a^2\rangle$, respectively) with further introduction of point defects. By contrast, there is a sharp increase in the value of $\langle\sigma^2\rangle$ (i.e., from $\sim\langle\sigma_a^2\rangle$ to $\langle\sigma_L^2\rangle$) and a corresponding decrease of G_d to zero when the crystal melts upon thermal heating.

E. The values of G_d calculated for the compounds FeTi, NiZr, and $NiZr_2$ are plotted versus $\langle\sigma^2\rangle$ in Fig. 6. For a direct comparison of the shear softening effect for different alloys, both G_d and $\langle\sigma^2\rangle$ have been normalized to the values of the perfect crystal (G_c) and the corresponding liquid ($\langle\sigma_L^2\rangle$), respectively. The data points obtained for isothermal disorder and isobaric heating lie within a narrow band, indicating that the dependence of G_d on $\langle\sigma^2\rangle$ or $\langle\mu_T^2\rangle$ is of a universal nature. The linear dependence of G_d on $\langle\sigma^2\rangle$ is consistent with the analytical model of Knuyt et

al.,[32] and the fact that isothermal amorphization and isobaric melting occur whenever $\langle\sigma^2\rangle/\langle\sigma_L^2\rangle$ reaches a critical value (between 0.5 and 0.6) provides a direct confirmation of the generalized Lindemann melting criterion for solid-state amorphization. .

Recently, Kulp et al.[35] have proposed that the distribution of the atomic-level shear stresses can be used as a criterion for amorphization. They showed that the crystal becomes amorphous when the average shear strain (calculated by dividing the average shear stress by two times the shear modulus) attains a critical value equal to that of the quenched-liquid state. This microscopic criterion is consistent with the generalized melting criterion discussed in the present work.

F. The Debye temperature θ_d was also determined from the average shear modulus G_d, using the well-known expression for isotropic media.[36] The variation of θ_d with damage dose is shown in Fig. 7 for NiZr and $NiZr_2$. The Debye temperature decreases rapidly from the initial value, θ_c, with increasing dose and saturates after the onset of amorphization. The calculated values of θ_c and θ_a were ~315 and 200 K for NiZr, and 260 and 180 K for $NiZr_2$, respectively. The corresponding measurements reported are 270 and 205 K, and 216 and 185 K for the two respective compounds.[37-39] Good agreement between the theoretical and experimental values is obtained for the glassy state, but discrepancies are noted for the defect-free crystalline state. Finally, the variation of the Debye temperature with increasing state of disorder as measured by $(1 - S^2)$ is illustrated in Fig. 8. The calculated θ_d^2 was found to decrease approximately linearly with $(1 - S^2)$, reaching the value of the amorphous compound when the c-a transition occurred.

2.4. Supporting Experimental Evidence

The generalized melting criterion is supported by numerous measurements. The obvious support is provided by the steeply-plunging polymorphous melting curves (T_o curves) of terminal solid solutions of many binary phase diagrams. Such curves are characteristic of large atomic size differences and extremely limited solute solubilities exhibited by easy glass-forming systems. In

fact, the Lindemann plot of T_d versus $\langle\mu_T^2\rangle$ represents a generalization of the T_o curves on binary phase diagrams, since the total static displacements provide a direct measure of the concentration of misfitting solute atoms. This plot is universal in the sense that it defines, in terms of a single parameter $\langle\mu_T^2\rangle$, the stability limits of defective crystals, supersaturated solid solutions, and chemically-disordered intermetallic compounds.

The predicted effect of static displacements on the Debye temperature is well supported by recent Brillouin scattering measurements on ion bombarded compounds,[4] which show that the square of the average sound velocity in the defective crystalline compound is a linerarly decreasing function of the quantity $(1 - S^2)$. An example is given in Fig. 9 for Kr^+ bombarded Zr_3Al.[6] The sound velocity becomes insensitive to further disorder when S has reached the critical value at which amorphization occurs. This result is consistent with the generalized Lindemann prediction (see Fig. 1), since the average sound velocity is proportional to the square root of the average shear modulus[40] and, as shown by our molecular dynamics simulations in Fig. 10 and by the experimental data in Fig. 11 for the case of quenched Cu_3Au,[41] the mean-square static displacement is a linear function of $(1 - S^2)$.

Another confirmation is illustrated in Fig. 12, based on the experimental work by Mirmel'shteyn et al.[42] on neutron-irradiated Mo_3Si. The squared Debye temperature of the damaged compound, θ_d^2, was found to decrease linearly with increasing $(1 - S^2)$. Below a critical state of disorder, corresponding to $S \approx 0.3$ where θ_d becomes equal to θ_a, the compound cannot be retained in the crystalline state.

The connection between a critical mean-square static displacement and the onset of amorphization can also be found in recent ion-implantation studies by Linker et al.[43-47] An example is shown in Fig. 13. As B ions were implanted into Nb, the average static displacement μ_s of the matrix atoms increased rapidly, reaching a maximum value for B concentrations of ~5 at.%. Incorporation of interstitial B solutes also led to a simultaneous increase in the lattice parameter and accumulation of strains. The onset of amorphization occurs when μ_s attains a critical, maximum value (~0.14 Å) and is accompanied by a significant strain release. Similar

features were also demonstrated for the amorphization process in Mn-implanted Al, a substitutional alloy system.[46,47] In this case, however, the lattice parameter *decreased* linearly with progressive incorporation of undersized Mn solutes until amorphization set in at a critical concentration of ~8 at.% Mn.

Recent *in situ* high-voltage electron-microscopy (HVEM) investigations showed that pre-doping the intermetallic compound Zr_3Al with small amounts of hydrogen caused a twenty-fold reduction in the electron dose necessary to amorphize the compound.[48] Hydrogen charging is itself capable of amorphizing this compound.[49] Thus, consistent with our prediction, hydrogen pre-doping introduces additional static displacements, which reduce the contribution from irradiation-induced defects needed to trigger amorphization.

3. ALLOY SUSCEPTIBILITY TO AMORPHIZATION

Equation (8) provides a thermo-elastic criterion for amorphization, which is based on the difference in the elastic properties of equilibrium intermetallic compounds and their glassy counterparts. Since the enthalpy difference between the crystalline and amorphous phases is proportional to the difference in their Debye temperatures, a compound can be expected to be more susceptible to defect-induced amorphization when the difference in the Debye temperatures is small. This prediction is confirmed by available measurements. Figure 14A, for example, shows the Debye temperatures measured for pure elements and several ordered compounds[37,38] and amorphous alloys[39,50,51] of the Ni-Zr system. The difference between the Debye temperatures of the crystalline and amorphous states is largest for Ni_3Zr, intermediate for NiZr and smallest for $NiZr_2$. The critical doses for amorphization of these compounds by electron irradiation were also measured[8,52] (Fig. 14B). Indeed, the critical electron dose near 0 K was found to be largest (3.18 dpa) for Ni_3Zr , intermediate (0.37 dpa) for NiZr and smallest (0.22 dpa) for $NiZr_2$.

Additional support for the thermo-elastic approach to solid-state amorphizing transformation is provided by the glass forming characteristics of binary alloy systems. T_0 curves on binary phase diagrams reflect not only the composition dependence of the free energies of the

solid and liquid phases but, according to the generalized Lindemann hypothesis, also reflect the compositional dependence of the average shear modulus and the Debye temperature of the crystalline state. As shown in Fig. 1, the intersection of the θ_d^2 curve and the θ_a^2 line defines a critical value, $<\mu_{cri}^2>^t$, of the mean-square static displacement beyond which the disordered crystal becomes thermodynamically unstable relative to the glass, i.e., $\Delta H_d < 0$. Since $<\mu_T^2>$ can represent the concentration of misfitting solute atoms, $<\mu_{cri}^2>^t$ is representative of a critical solute concentration for glass formation. An example is presented in Fig. 15 for the Zr-Rh binary system. The minimum Rh concentration required to for glass formation by rapid solidification techniques has been found to be ~15 at% .[53] This minimum concentration lies very close to where the steeply plunging Debye temperature curve for the Zr-rich terminal solid solution[54] intersects the relatively flat Debye temperature vs. composition curve determined for the amorphous phases.[55-60] The intersection point defines the critical Rh concentration beyond which the crystalline solid solution becomes energetically unstable relative to the amorphous state.

4. CRITICAL TEMPERATURE FOR AMORPHIZATION AND KINETIC EFFECTS

One of the strongest experimental support of the generalized Lindemann melting criterion is provided by studies on Zr_3Al,[4,6] which show that during irradiation the onset of amorphization occurs when the average shear modulus of the defective compound becomes equal to that of the amorphous phase. This elasticity criterion for amorphization is essentially a thermodynamic criterion that follows directly from eq. (9), which shows that the enthalpy difference between the amorphous phase and the defective crystal vanishes when their average shear moduli, as measured by Debye temperatures, become equal. As shown schematically in Fig. 1, this thermo-elastic criterion for amorphization defines an upper-limiting temperature for amorphization, T_a, since a thermodynamic driving force for amorphization, i.e., $\Delta H_d \leq 0$, exists only for temperatures below T_a. The extension of the generalized Lindemann melting criterion to the amorphous phase implies that T_a is the melting temperature of the amorphous phase, which can be interpreted as the glass transition temperature, T_g. Indeed, when $\theta_d = \theta_a$, it follows from eq. (5) that

$$\frac{T_g}{T_m} = \frac{\theta_a^2}{\theta_c^2} = t_g \qquad (11)$$

where t_g is the reduced glass transition temperature. This relationship has been experimentally verified for Cu-Zr glasses.[57]

Additional support is also provided by Fig. 16 showing that the upper-limiting temperature for radiation-induced amorphization of the CuTi compound is $T_a \simeq 575$ K, [61] which is close to the crystallization temperature determined by slow, continuous heating of amorphous Cu-Ti ribbons[62] and by isochronal annealing of irradiated and unirradiated amorphous $Cu_{64}Ti_{36}$ alloys.[63] T_a has also been determined recently for NiAl and NiTi, 240 and 600 K respectively.[64] Furthermore, Fig. 16 reveals a number of important features: (i) At sufficiently low temperatures where amorphization occurs homogeneously, the critical dose for amorphization is independent of temperature and of the type of irradiating particles, and ; (ii) For any given type of particles, there is a critical temperature T^* above which the compound cannot be completely amorphized; and (iii) For similar dose rates, T^* increases with the particle mass, asymptotically approaching the value of T_a. These results clearly demonstrate the importance of kinetic effects. For example, the value of $T^* \simeq 220$ K for electron-induced amorphization has been shown to be equal to the temperature at which the long-range order parameter abruptly decreases from 1 to ~0.2.[8] The Zee-Wilkes model[65] of radiation-induced order-disorder transformation predicts that T^* for electron irradiation is determined mainly by the defect production rate and the migration energy of the mobile defects that tend to restore long-range order. For the defect-production rates employed experimentally, Xu[8] has shown that a defect migration energy of ~0.6 eV was required to account for the observed T^*. This value is remarkably close to the energies of 0.60 - 0.75 eV calculated by molecular statics for vacancy migration across the {002} Ti planes in partially-disordered CuTi compound.[66] These vacancy jumps are responsible for restoring long-range order in this structure. In contrast to the electron case, the temperature T^* measured for heavy ions such as Kr and Xe has been shown to be the temperature at which small amorphous zones embedded in a crystalline matrix become

unstable with respect to crystallization via growth of the crystalline phase, i.e., crystallization without nucleation events.[7,61]

It was also found that the mode of amorphization changed with irradiation temperature. Near T^* for electron irrradiation, the amorphous phase nucleated heterogeneously at dislocations, grain boundaries, and free surfaces; interfaces between the amorphous zones and the crystalline matrix were well defined.[3,67] At temperatures well below T^*, however, the c-a transition occured homogeneously within the entire irradiated volume, despite the presence of extended defects.[4,61,68]

5. CONCLUSION

The present communication focuses on mechanistic aspects of the solid-state amorphizing transformation. We propose that this transition can be viewed a disorder-induced melting of metastable crystals. By considering static atomic displacements as a generic measure of chemical and topological disorder in solids, a unified description of solid-state amorphization was developed on the basis of a generalized form of the well-known Lindemann melting criterion. The generalized version assumes that melting of a defective crystal occurs whenever the sum of the thermal and static displacements reaches a critical value identical to that for melting of the defect-free crystal. The thermodynamic equivalence between thermal and static displacements implied by the criterion is consistent with the diffraction analysis of diffuse scattering from disordered crystal where the effect of static displacements appears as artificially-enlarged Debye-Waller factor.

Our molecular-dynamics studies of amorphization and melting have, however, shown that the equivalence between static and thermal disorder extends beyond diffraction effects per se. For example, plots of the average shear modulus versus $\langle\mu_T^2\rangle$ appear identical for the following processes: isobaric heating to melting of the perfect long-range ordered structure, in which $\langle\mu_T^2\rangle = \langle\mu_{vib}^2\rangle$, and progressive atomic disordering at low temperature where $\langle\mu_T^2\rangle \approx \langle\mu_{sta}^2\rangle$. For both processes, the average shear modulus was found to decrease essentially linearly with increasing $\langle\mu_T^2\rangle$, and the threshold values of $\langle\mu_T^2\rangle$ were the same. These results demonstrate that $\langle\mu_T^2\rangle$

provides a direct measure of the potential energy stored in the lattice. Hence, it can be used as a generalized disorder parameter in a unified thermodynamic approach to melting and solid-state amorphization. An important prediction of this criterion is that the melting temperatrure of a defective crystal must decrease with increasing disorder, which in turn implies the existence of a critical state of disorder beyond which the melting temperature falls below the glass transition temperature. The generalized Lindemann criterion therefore leads to a natural interpretation of c-a transformations as melting to a glass of a critically-disordered crystal. The predicted effect of static displacements on the Debye temperarure has been supported by various measurements of radiation-induced amorphization. In addition, the generalized Lindemann criterion successfully accounts for a large number of experimental observations, including (i) why some intermetallic compounds are more susceptible to amorphization than others, (ii) why the onset of amorphization occurs when the average sound velocity in the irradiated compound becomes equal to that of the fully amorphous state, (iii) why the projectile-mass-dependent critical temperature for radiation-induced amorphization approaches an upper-limiting value which is close to the experimentally-observed glass transition temperature, and (iv) the existence of a minimum solute concentration for glass formation by rapid quenching, by ion implantation, or by ion-beam mixing. Due to its independence of the physical origin of $\langle \mu_T^2 \rangle$, the generalized Lindemann melting criterion provides not only the parallel between amorphization and isobaric melting, but also a basic link between the various solid-state amorphizing transformations.

ACKNOWLEDGMENTS

The authors are grateful to Dr. L.E. Rehn for stimulating discussions and continued interest. This work was supported by the U.S. Department of Energy, Basic Energy Sciences-Materials Sciences, under contract W-31-109-Eng-38, and by the National Science Foundation, under Grant DMR-8802847. It benefited from an allocation of computer time on the Cray system at the National Energy Research Supercomputer Center (Lawrence Livermore National Laboratorty).

REFERENCES

1. H. Wiedersich and M. Meshii (eds), *Science of Advanced Materials* (ASM International, Metals Park, OH, 1990).
2. G.J.C. Carpenter and E.M. Schulson, J. Nucl. Mater. **23**, 180 (1978).
3. H. Mori and H. Fujita, Japanese J. Appl. Phys. **21**, L494 (1982); G. Thomas, H. Mori, H. Fujita, and R. Sinclair, Scripta Metall. **16**, 589 (1982); H. Mori, H. Fujita and M. Fujita, Japanese J. Appl. Phys. **22**, L94 (1983); H. Mori, H. Fujita, M. Tendo, and M. Fujita, Scripta Metall. **18**, 783 (1984).
4. P.R. Okamoto and M. Meshii, in *Science of Advanced Materials*, edited by H. Wiedersich and M.Meshii (American Society for Metals, Metals Park,OH, 1990) p. 33. .
5. D.E. Luzzi, H. Mori, H. Fujita and M. Meshii, Acta Metall. **34**, 629 (1986).
6. P.R. Okamoto, L.E. Rehn, J. Pearson, R. Bhadra, and M. Grimsditch, J. Less Common Met. **140**, 231 (1988).
7. J. Koike, Ph.D. Thesis, Northwestern University, Evanston, IL (1989).
8. G. Xu, Ph.D. Thesis, Northwestern University, Evanston, IL (1993).
9. J. Koike, P.R. Okamoto, R.E. Rehn and M. Meshii, Mat. Res. Soc. Symp. Proc. **157**, 777 (1990).
10. A. Lindemann, Z. Phys. **11**, 609 (1910).
11. J.M. Ziman, *Principles of the Theory of Solids* (Cambridge University Press, Cambridge, 1972).
12. A. Voronel, S. Rabinovich, and A. Kisliuk, Phys. Rev. Lett. **60**, 2402 (1988).
13. A.P. Miodownik, in *Structural and Phase Stability of Alloys,* edited by J.L. Morán-López et al. (Plenum Press, New York, 1992) p. 65.
14. M.J. Sabochick and N.Q. Lam, Phys. Rev. **B43**, 5243 (1991).
15. N. Q. Lam, P. R. Okamoto, M. J. Sabochick, and R. Devanathan, J. Alloys and Compounds **194**, 429 (1993).

16. N. Q. Lam, P. R. Okamoto, R. Devanathan, and M. Meshii, Proceedings of the NATO Advanced Study Institute on *Statics and Dynamics of Alloy Phase Transformations*, June 21 - July 3, 1992, Rhodes, Greece (Plenum Press, New York) in press.

17. R. Devanathan, N. Q. Lam, M. J. Sabochick, P. R. Okamoto, and M. Meshii, J. Alloys and Compounds **194**, 447 (1993).

18. R. Devanathan, N. Q. Lam, P. R. Okamoto, and M. Meshii, Phys. Rev. **B48**, 42 (1993).

19. M. J. Sabochick and N. Q. Lam, Mat. Res. Soc. Symp. Proc. **201**, 387 (1991).

20. C. Massobrio, V. Pontikis, and G. Martin, Phys. Rev. **B41**, 10486 (1990).

21. H. Mori, H. Fujita, M. Tendo, and M. Meshii, Scripta Metall. **18**, 783 (1984).

22. H. Hsieh and S. Yip, Phys. Rev. **B39**, 7476 (1989).

23. C. Massobrio and V. Pontikis, Phys. Rev. **B45**, 2484 (1992)

24. M.F. Ashby, A.N. Nelson, and R.M.A. Centamore, Scripta Met. **4**, 715 (1970).

25. B. Golding, B.G. Bagley, and F.S.L. Hsu, Phys. Rev. Lett. **29**, 68 (1972).

26. J. Logan and M.F. Ashby, Acta Metall. **22**, 1047 (1974).

27. M.D. Merz, R.P. Allen, and S.D. Dahlgren, J. Appl. Phys. **45**, 4126 (1974).

28. J.J. Gilman, Phys. Today (May), 46 (1975).

29. C.P. Chou, L.A. Davis, and R. Hasegawa, J. Appl. Phys. **50**, 3334 (1979).

30. D. Weaire, M.F. Ashby, J. Logan, and M.J. Weins, Acta Metall. **19**, 779 (1971).

31. G. Knuyt, L. De Schepper, and L.M. Stals, J. Phys. F: Met. Phys. **16**, 1989 (1986).

32. G. Knuyt and L.M. Stals, Philos. Mag. **B64**, 299 (1991).

33. D. Wolf, P.R. Okamoto, S. Yip, J.F. Lutsko and M. Kluge, J. Mater. Res. **5**, 286 (1990).

34. E. Sevillano, H. Meuth, and J.J. Rehr, Phys. Rev. **B20**, 4908 (1979).

35. D.T. Kulp, T. Egami, D.E. Luzzi, and V. Vitek, J. Alloys and Compounds **194**, 417 (1993).

36. G. Busch and H. Schade, *Lectures on Solid State Physics* (Pergamon Press, New York, 1976) pp. 61-65.

37. A. Amamou, R. Kuentzler, Y. Dossmann, P. forey, J.L. Glimois, and J.L. Feron, J. Phys. F: Met. Phys. **12**, 2509 (1982).

38. D.G. Onn, L.Q. Wang, Y. Obi, and K. Fukamichi, Solid State Commun. **46**, 37 (1983).

39. M. Matsuura and U. Mizutani, J. Phys. F: Met. Phys. **16**, L183 (1986).

40. G. Grimvall, *Thermophysical Properties of Materials* , Selected Topics in Solid State Physics, Vol. XVIII (North-Holland, Amsterdam, 1986) pp. 37-44.

41. E.V. Kozlov, V.M. Dementryev, V.N. Emelyanov, N.M. Kormin, A.S. Taylashev, and D.M. Stern, in *Order-Disorder Transformation in Alloys*, edited by H. Warlimont (Springer-Verlag, Berlin, 1974) p. 58.

42. A.V. Mermel'shteyn, A.Ye. Kar'kin, V.Ye. Arkhipov, and V.I. Voronin, Phys. Met. Metall. **55**, 67 (1983).

43. G. Linker, Mater. Sci. Eng. **69**, 105 (1985).

44. G. Linker, Solid State Commun.. **57**, 773 (1986).

45. G. Linker, Nucl. Instrum. Methods **B19-20**, 526 (1987).

46. A. Seidel, S. Massing, B. Strehlau, and G. Linker, Phys, Rev. **B38**, 2273 (1988).

47. A. Seidel, G. Linker, and O. Meyer, J. Less-Common Met. **145**, 89 (1988).

48. W.J. Meng, J. Koike, P.R. Okamoto, and L.E. Rehn, Mat. Res. Soc. Symp. Proc. **128**, 345 (1989).

49. W.J. Meng, P.R. Okamoto, and L.E. Rehn, in *Science of Advanced Materials*, edited by H. Wiedersich and M.Meshii (American Society for Metals, Metals Park, OH, 1990) p. 99.

50. R. Kuentzler, J. Phys. F: Met. Phys. **14**, L79 (1984).

51. S. Kanemaki, O. Takehira, K. Fukamichi, and U. Mizutani, J. Phys.: Condens. Matter **1**, 5903 (1989).

52. G. Xu, M. Meshii, P.R. Okamoto, and L.E. Rehn, J. Alloys and Compounds **194**, 401 (1993).

53. X.L. Yeh and W.L. Johnson, Mat. Res. Soc. Symp. Proc. **58**, 63 (1986).

54. R. Kuentzler and R.M. Waterstrat, Solid State Commun. **54**, 517 (1985).

55. P. Garoche and W.L. Johnson, Solid State Commun. **39**, 403 (1981).

56. W. Eschner and W. Gey, in *Superconductivity in d- and f-band Metals*, edited by W. Buckel and W. Weber (Kernforschungszentrum, Karlsruhe, 1982) p. 329.

57. P. Garoche and J. Bigot, Phys. Rev. **B28**, 6886 (1983).

58. R. Kuentzler, A. Amamou, R. Clad, and P. Turek, J. Phys. F: Met. Phys. **17**, 459 (1987).

59. D.G. Onn, L.Q. Wang, and K. Fukamichi, Solid State Commun. **47**, 479 (1983).

60. S. Roy and A.K. Mandale, J. Phys. F: Met. Phys. **18**, 2649 (1988).

61. J. Koike, P.R. Okamoto, R.E. Rehn and M. Meshii, J. Mater. Res. **4**, 1143 (1989).

62. T.B. Massalski and C.G. Woychik, Acta Metall. **33**, 1873 (1985).

63. G. Schumacher, S. Klaumünzer, W. Petry, and U. Dedek, J. Phys. F: Met. Phys. **18**, 1681 (1988).

64. P. Moine and C. Jaouen, J. Alloys Comp. **194**, 373 (1993).

65. R. Zee and P. Wilkes, Phil. Mag. **42**, 463 (1980).

66. J.R. Shoemaker, R.T. Lutton, D. Wesley, W.R. Wharton, M.L. Oehrli, M.S. Herte, M.J. Sabochick, and N.Q. Lam, J. Mater. Res. **6**, 473 (1991).

67. H. Fujita, H. Mori, and M. Fujita, Proc. Seventh Int. Conf. on *High Voltage Microscopy* , Berkeley, 1983, edited by R.M. Fisher, R. Gronsky, and K.H. Westmacott, p. 233.

68. D.E. Luzzi and M. Meshii, Res Mechanica **21**, 207 (1987).

FIGURE CAPTIONS

Fig. 1: Predicted dependence of the Debye temperature, average shear modulus, instability temperature, and enthalpy of crystallization on total mean-square atomic displacement, based on the generalized Lindemann melting criterion. $\langle\mu^2_{cri}\rangle^t$ and $\langle\mu^2_{cri}\rangle^m$ denote the critical values of $\langle\mu^2_T\rangle$ for *thermodynamic* and *mechanical* melting, respectively.

Fig. 2: Increases in the potential energy and volume of NiZr as a result of increasing number of atom exchanges or Frenkel pairs per atom, and evolution of the compound microstructure as characterized by progressive changes in pair-correlation function g(r), [100] diffraction pattern, and projection of atom positions onto the (100) plane.

Fig. 3: Plots of the average shear modulus G_d versus the volume expansion $\Delta V/V$, mean-square atomic displacement $\langle\mu^2_T\rangle$, and mean-square dispersion in the nearest-neighbor distance $\langle\sigma^2\rangle$ in NiZr. The variation of $\langle\mu^2_T\rangle$ with $\Delta V/V$ is also shown for the cases of ordinary melting and chemical disordering. The solid and dashed arrows indicate the occurrence of amorphization in the defective compound and the state of the defect-free crystal just below its melting point (1400 K), respectively.

Fig. 4: Variations of the average shear modulus G_d with the volume expansion $\Delta V/V$, mean-square atomic displacement $\langle\mu^2_T\rangle$, and mean-square dispersion in the nearest-neighbor distance $\langle\sigma^2\rangle$ in $NiZr_2$. The increase in $\langle\mu^2_T\rangle$ with $\Delta V/V$ caused by melting and chemical disordering is also shown. The solid and dashed arrows correspond to the onset of amorphization in the defective compound and the defect-free crystal at ~50 K below its melting point (1500 K), respectively.

Fig. 5: Linear relationship between the mean-square amplitude of thermal vibrations $\langle\mu^2_{vib}\rangle$ and the mean-square dispersion in the nearest-neighbor distance $\langle\sigma^2\rangle$ in NiZr and $NiZr_2$.

Fig. 6: Variation of the average shear modulus with the mean-square dispersion in the nearest-neighbor distance in the compounds FeTi, NiZr and $NiZr_2$. The shear modulus G_d has been normalized to the value obtained of the perfect crystal G_c, and $\langle\sigma^2\rangle$ normalized to its value in the liquid $\langle\sigma^2_L\rangle$.

Fig. 7: Damage-dose dependence of the Debye temperature θ_d calculated for NiZr and $NiZr_2$. The experimental values for the undamaged crystalline compounds [37] and glassy alloys [38] are indicated.

Fig. 8: Dependence of the Debye temperature θ^2_d on state of disorder $(1 - S^2)$ in NiZr and $NiZr_2$. S is the Bragg-Williams long-range order parameter. The experimental values of θ^2_d for the glassy alloys [38] are indicated.

Fig. 9: Decrease of the average sound velocity with increasing state of disorder $(1 - S^2)$ in 1-MeV Kr^+ bombarded Zr_3Al. After Okamoto et al. [6].

Fig. 10: Linear relationship between the normalized $\langle\sigma^2\rangle$ and $(1 - S^2)$ obtained in simulations of NiZr and $NiZr_2$.

Fig. 11: Linear relationship between $\langle\mu^2_T\rangle$ and $(1 - S^2)$ measured on quenched Cu_3Au. After Kozlov et al. [41].

Fig. 12: Linear relationship between θ^2_d and $(1 - S^2)$ measured on neutron-irradiated Mo_3Si. After Mirmel'shteyn et al. [42].

Fig. 13: Plots of the average static atomic displacement μ_s, lattice parameter, and volume fraction of the amorphized material versus the concentration of B atoms implanted into Nb. After Linker [43].

Fig. 14: (A) Compositional dependence of the Debye temperature measured for the Ni-Zr alloy system. Data for pure elements and ordered compounds are taken from refs. 37,50, and data for amorphous alloys from refs. 38,39,51. (B) Temperature dependence of the critical dose for amorphization of NiZr, $NiZr_2$, and Ni_3Zr. After Xu et al. [52].

Fig. 15: Compositional dependence of the Debye temperature measured for the Zr-Rh alloy system. Data for pure elements, crystalline solid solutions, and ordered compounds are taken from ref. 54, and data for amorphous alloys from refs. 55-60.

Fig. 16: Temperature dependence of the critical dose for amorphization of the compound CuTi during irradiation with electrons, Ne^+, Kr^+, and Xe^+ ions. After Koike et al. [61].

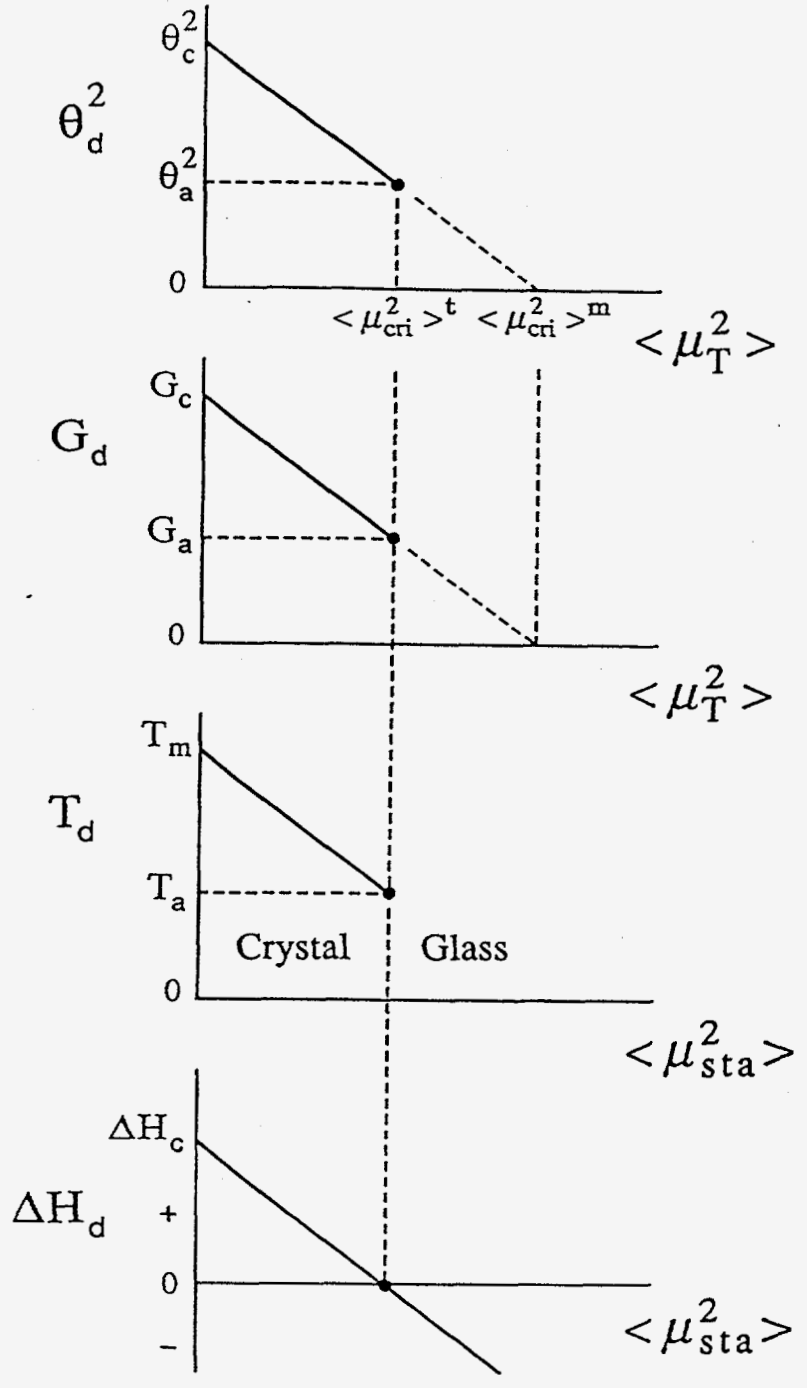

Fig. 1 (N. Q. Lam et al.

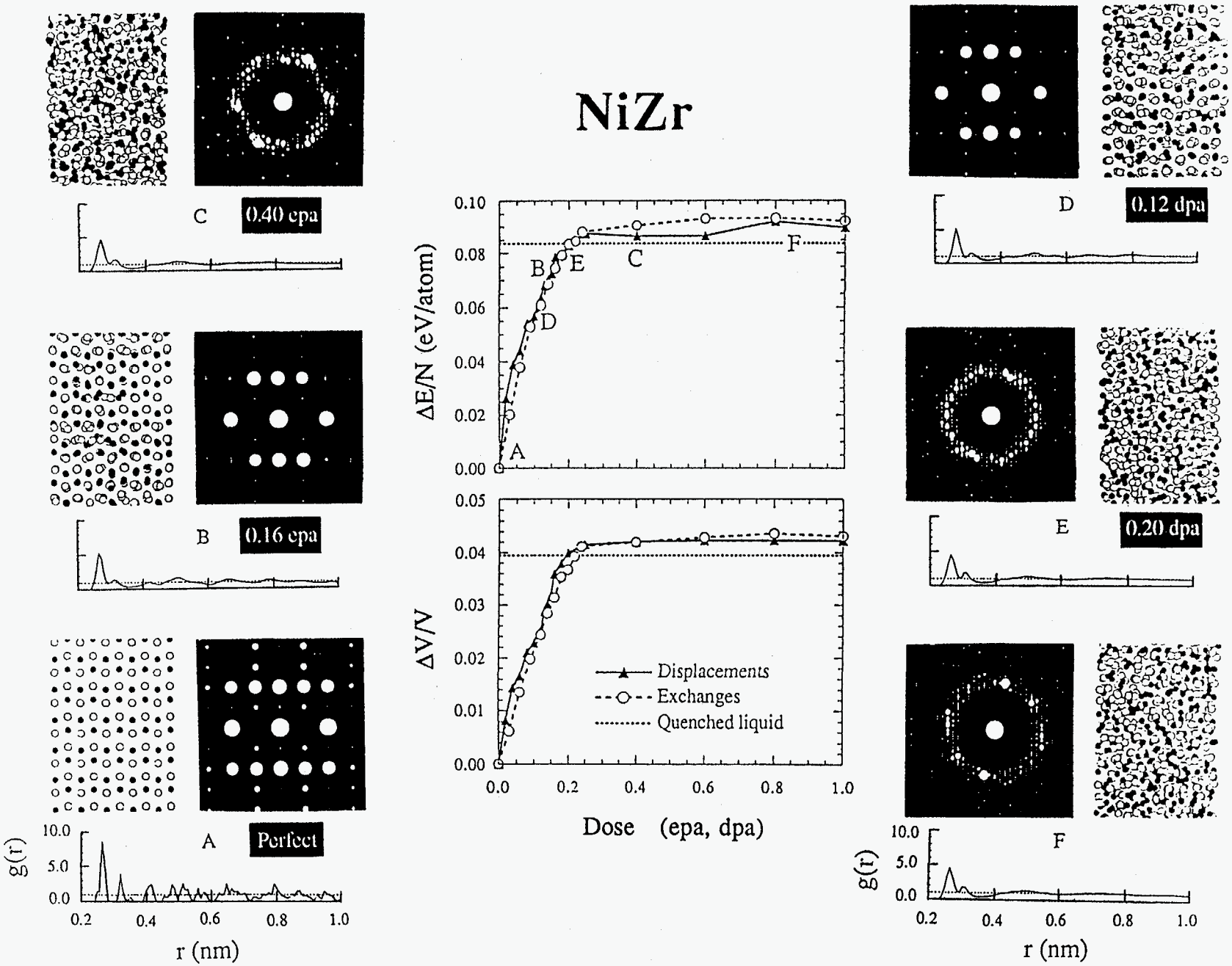
NiZr
C
0.40 epa
B
0.16 epa
A
Perfect
g(r)
10.0
5.0
0.0
0.2
0.4
0.6
0.8
1.0
r (nm)
ΔE/N (eV/atom)
0.10
0.08
0.06
0.04
0.02
0.00
A
B
C
D
E
F
ΔV/V
0.05
0.04
0.03
0.02
0.01
0.00
Displacements
Exchanges
Quenched liquid
0.0
0.2
0.4
0.6
0.8
1.0
Dose (epa, dpa)
D
0.12 dpa
E
0.20 dpa
F
g(r)
10.0
5.0
0.0
0.2
0.4
0.6
0.8
1.0
r (nm)

Fig. 2

NiZr

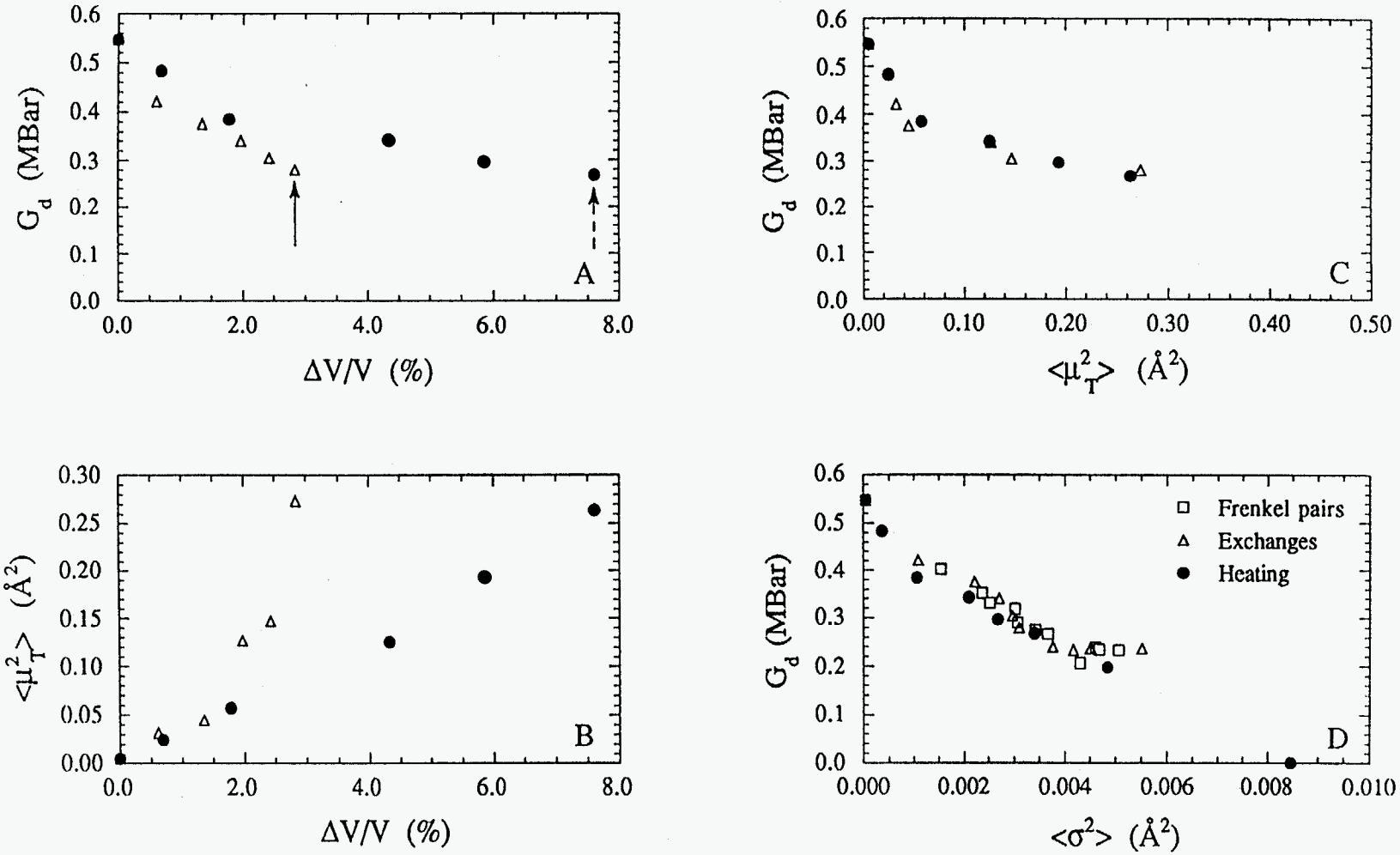
G_d (MBar)
$\Delta V/V$ (%)
A
$\langle \mu^2_T \rangle$ (Å^2)
B
C
$\langle \sigma^2 \rangle$ (Å^2)
D
Frenkel pairs
Exchanges
Heating

Fig. 3

$NiZr_2$

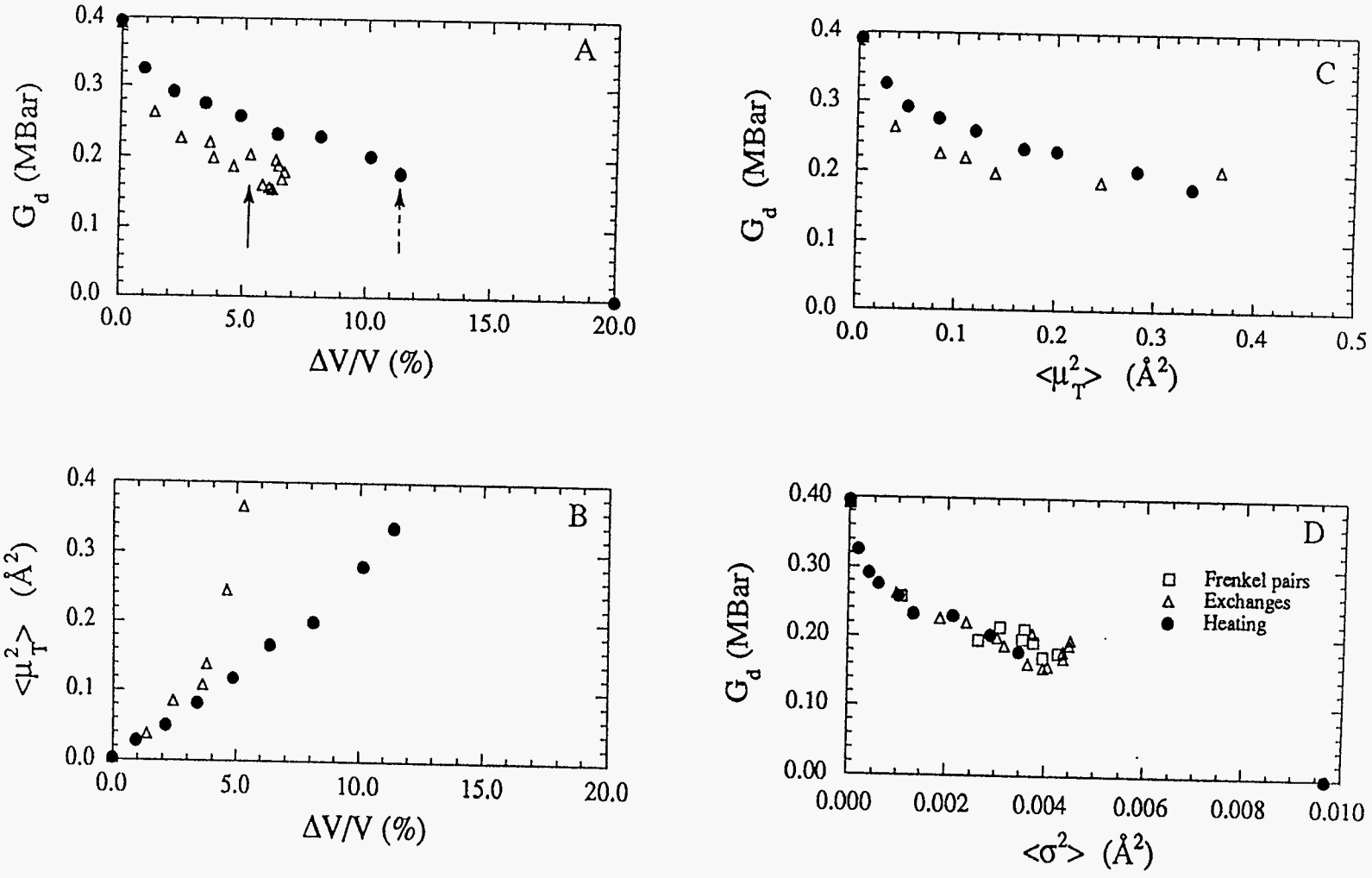
A
G_d (MBar)
$\Delta V/V$ (%)
B
$\langle \mu_T^2 \rangle$ (Å^2)
$\Delta V/V$ (%)
C
G_d (MBar)
$\langle \mu_T^2 \rangle$ (Å^2)
D
G_d (MBar)
$\langle \sigma^2 \rangle$ (Å^2)
Frenkel pairs
Exchanges
Heating

Fig. 4

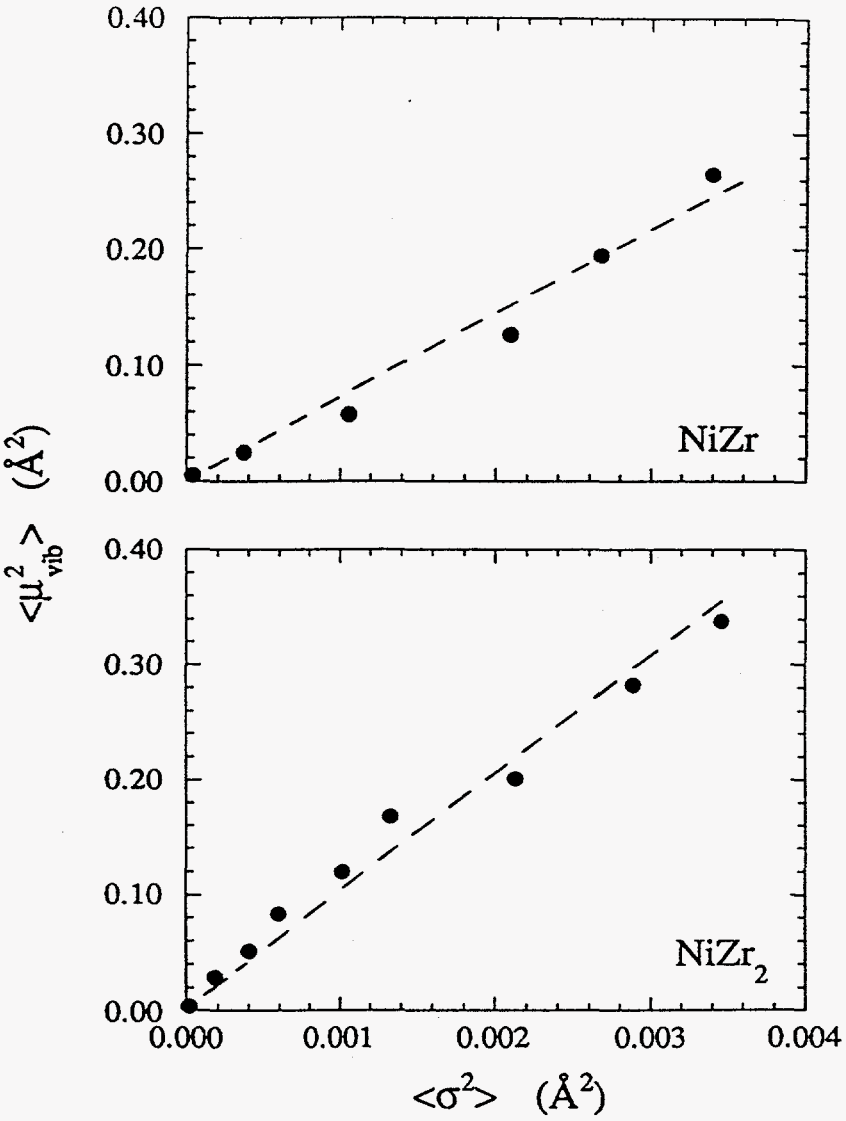
0.40
0.30
0.20
0.10
0.00
NiZr
0.40
0.30
0.20
0.10
0.00
NiZr2
0.000
0.001
0.002
0.003
0.004
<μ2vib> (Å2)
<σ2> (Å2)

Fig. 5

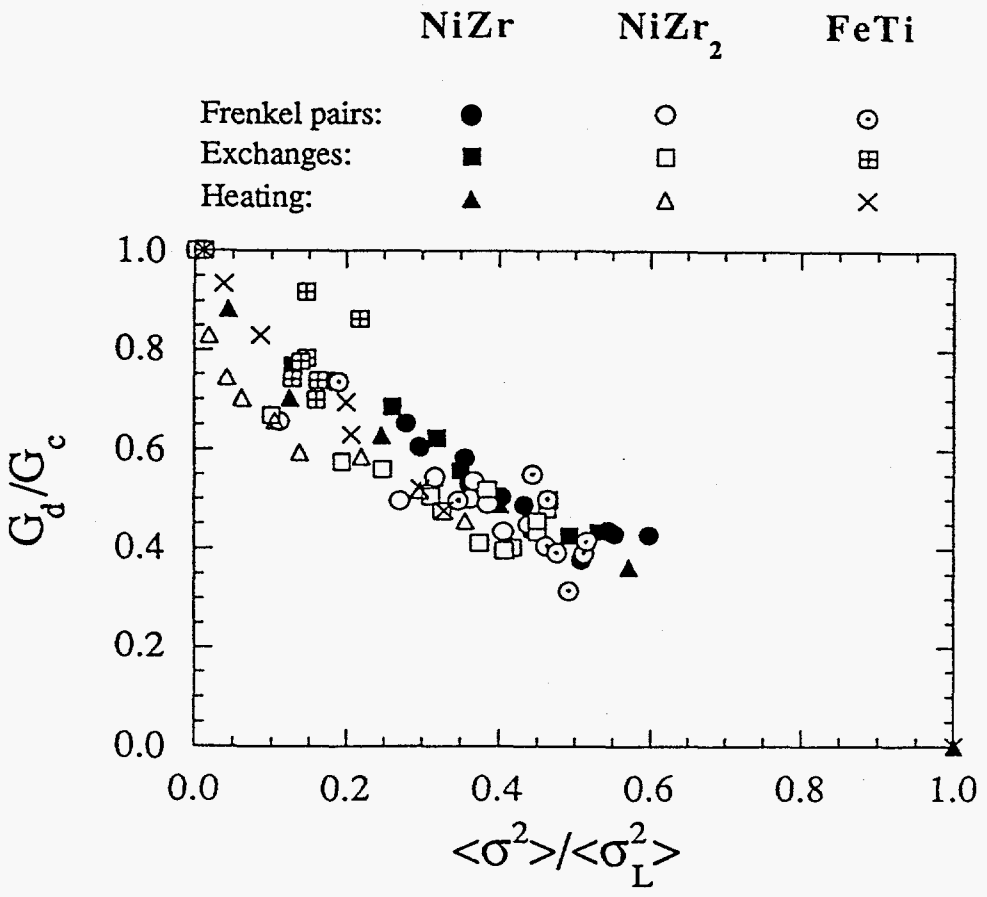
NiZr
NiZr2
FeTi
Frenkel pairs:
Exchanges:
Heating:
1.0
0.8
0.6
0.4
0.2
0.0
0.0
0.2
0.4
0.6
0.8
1.0
Gd/Gc
<σ2>/<σ2L>
Fig. 6

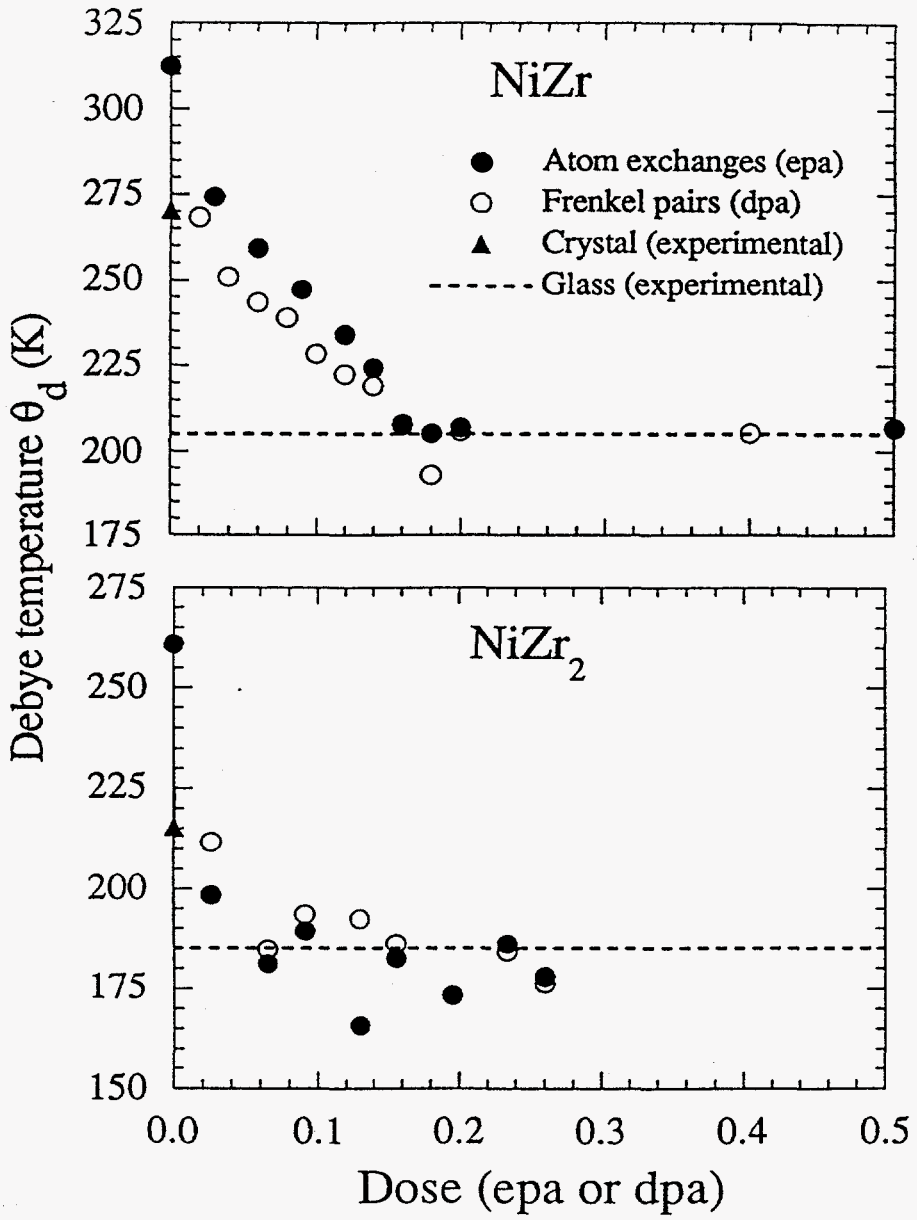

Fig. 7 (N.Q. Lam et al.)

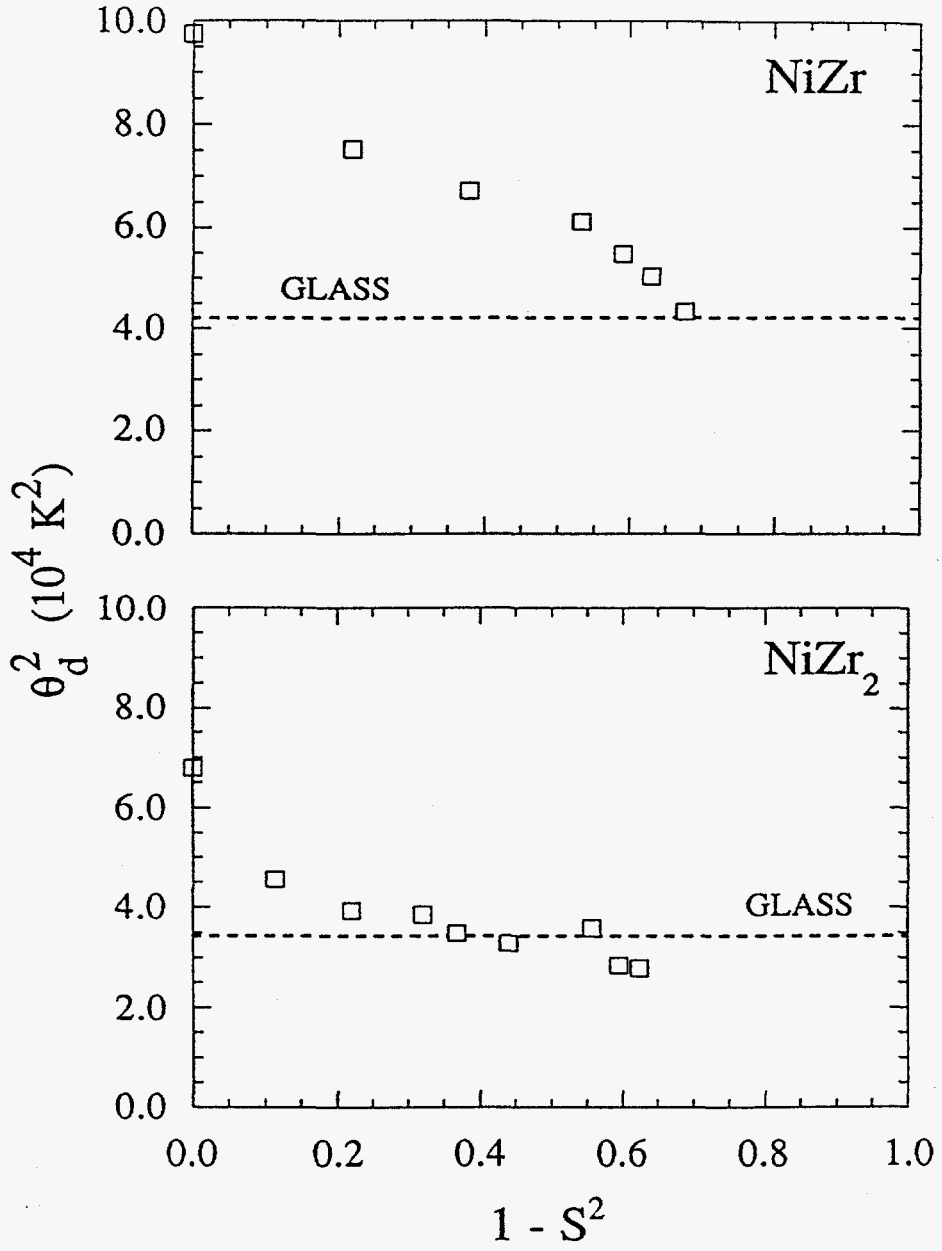

Fig. 8 (N. Q. Lam et al.)

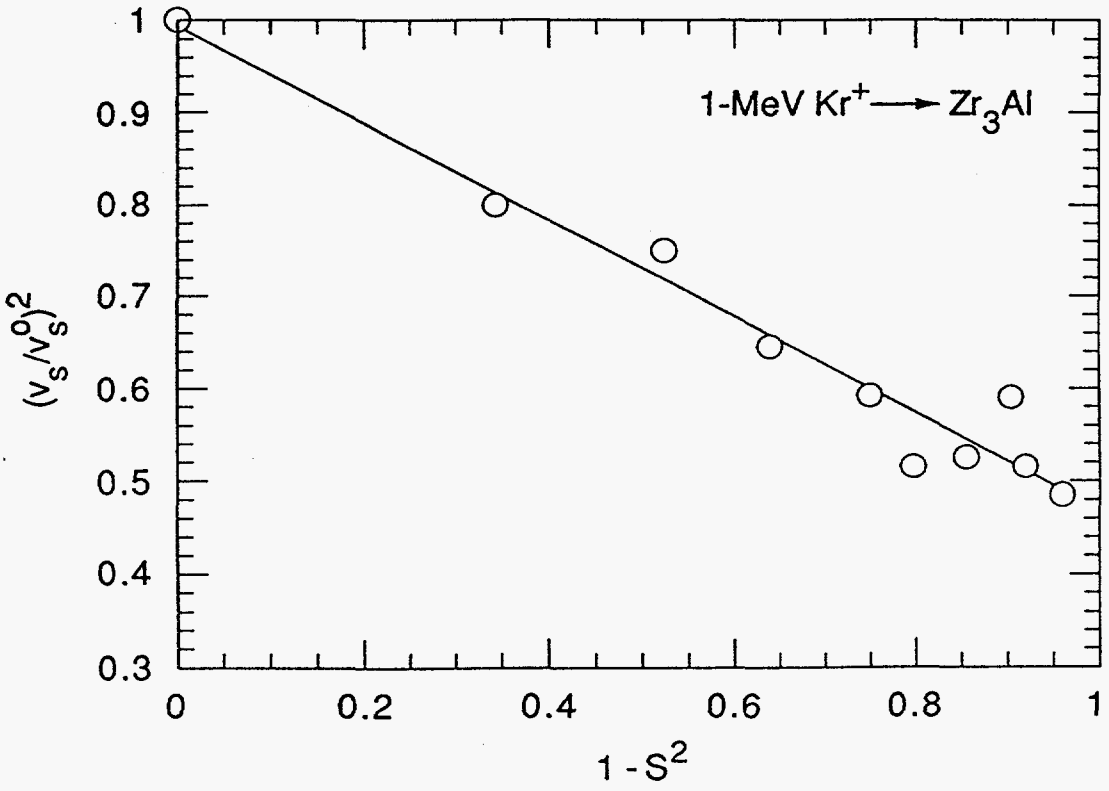
1-MeV $Kr^+ \rightarrow Zr_3Al$
$(v_s/v_s^0)^2$
$1 - S^2$
1
0.9
0.8
0.7
0.6
0.5
0.4
0.3
0
0.2
0.4
0.6
0.8
1

Fig. 9

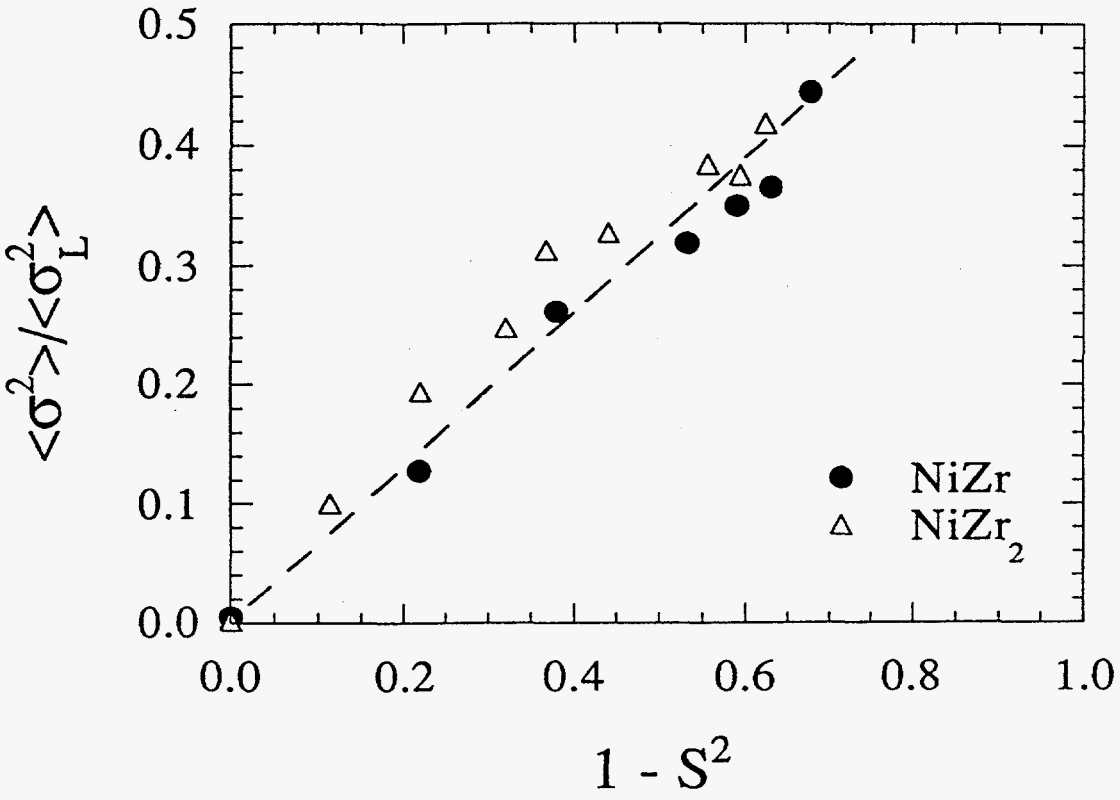
0.5
0.4
0.3
0.2
0.1
0.0
0.0
0.2
0.4
0.6
0.8
1.0
$\langle\sigma^2\rangle/\langle\sigma_L^2\rangle$
$1 - S^2$
NiZr
$NiZr_2$

Fig. 10

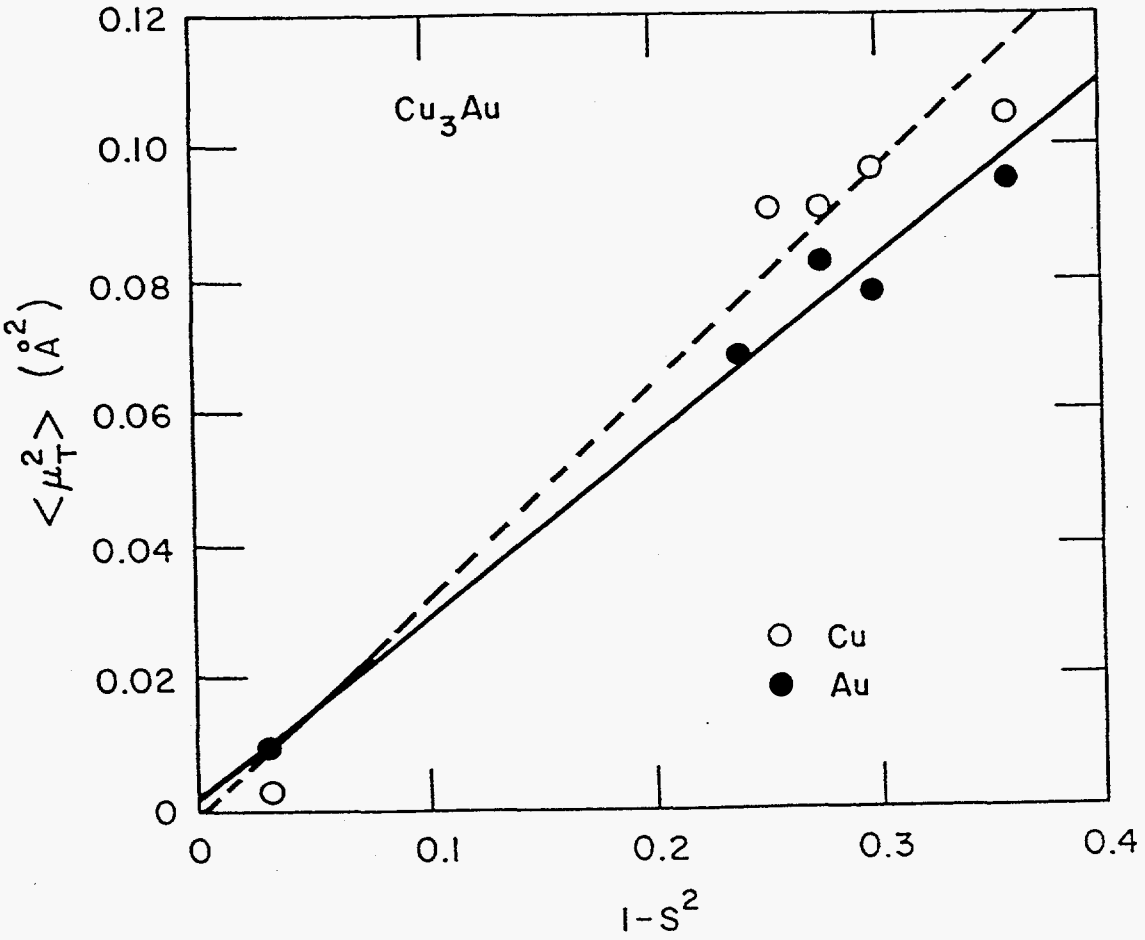
0.12
0.10
0.08
0.06
0.04
0.02
0
$\langle \mu_T^2 \rangle$ ($\AA^2$)
Cu_3Au
Cu
Au
0
0.1
0.2
0.3
0.4
$1-s^2$

Fig. 11

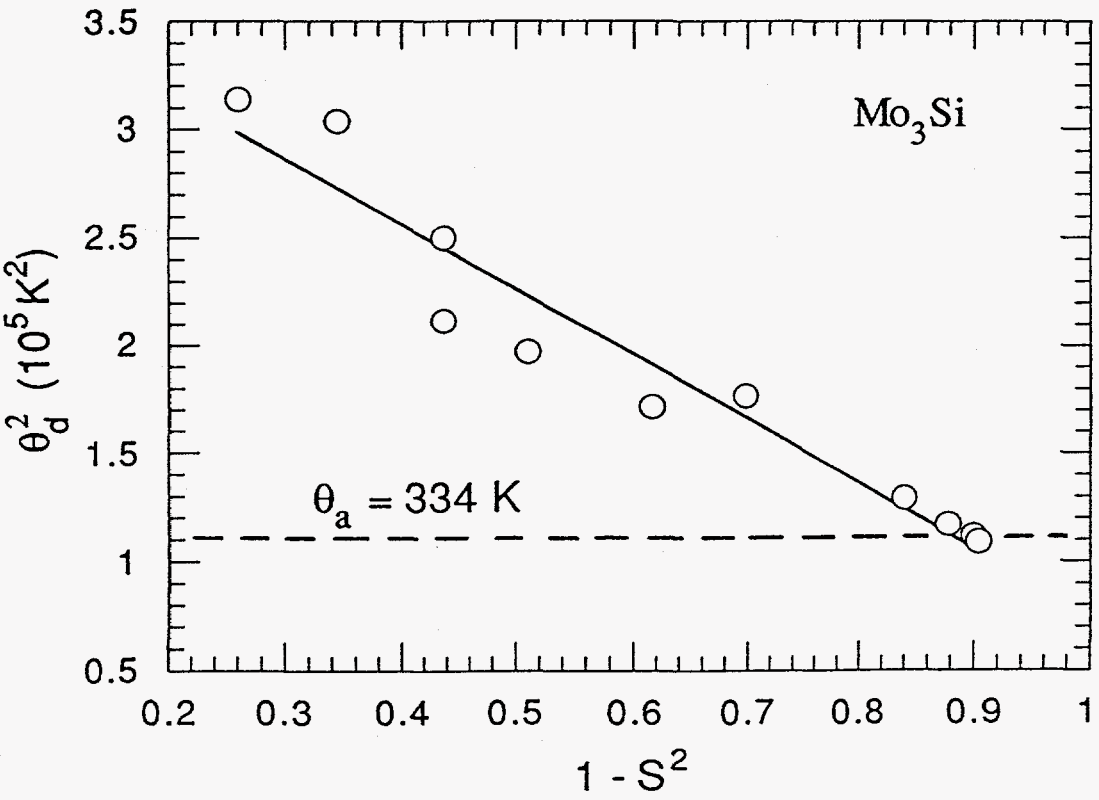
3.5
3
2.5
2
1.5
1
0.5
θ_d^2 (10^5 K^2)
Mo_3Si
θ_a = 334 K
0.2
0.3
0.4
0.5
0.6
0.7
0.8
0.9
1
1 - S^2

Fig. 12

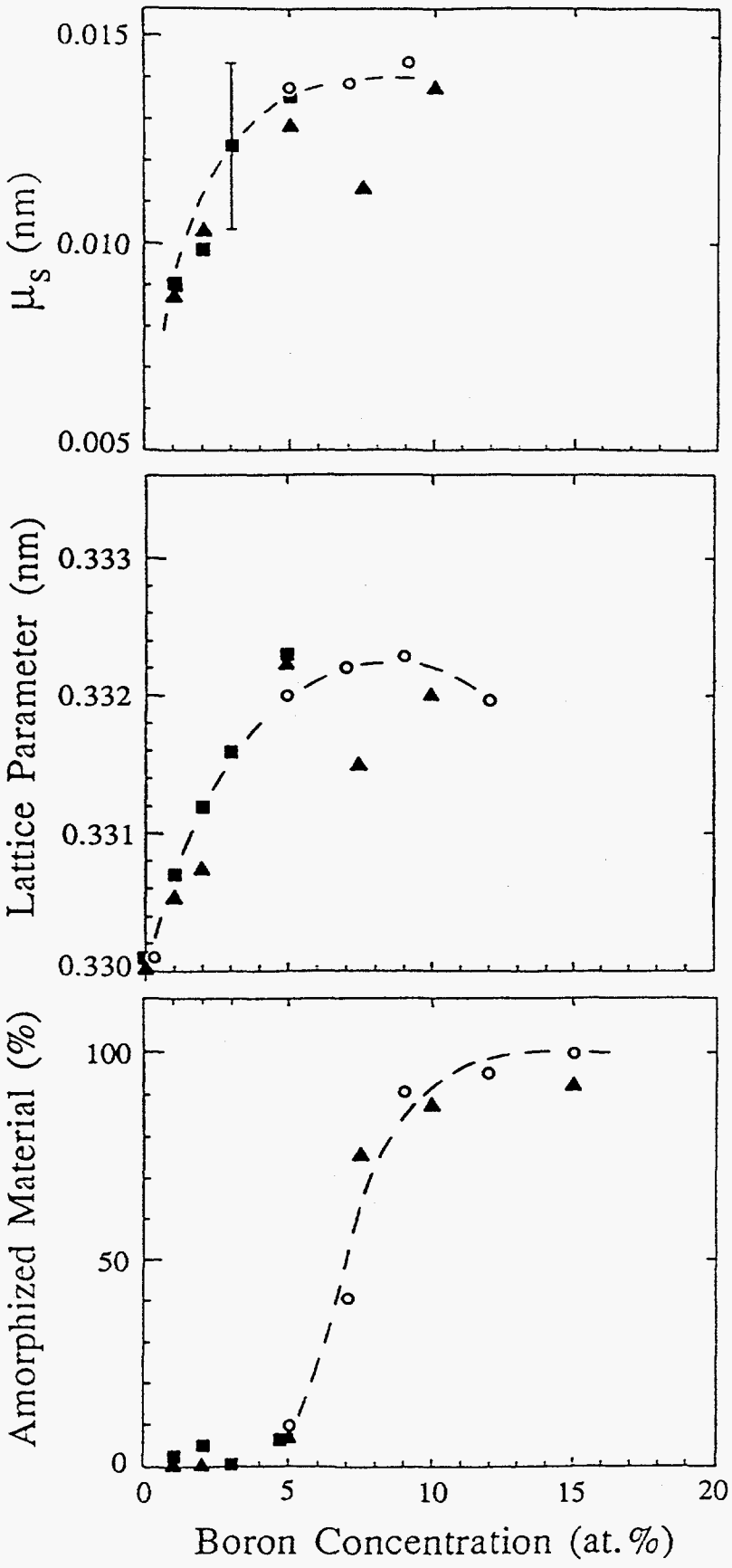
0.015
0.010
0.005
μ_s (nm)
0.333
0.332
0.331
0.330
Lattice Parameter (nm)
100
50
0
Amorphized Material (%)
0
5
10
15
20
Boron Concentration (at.%)

Fig. 13

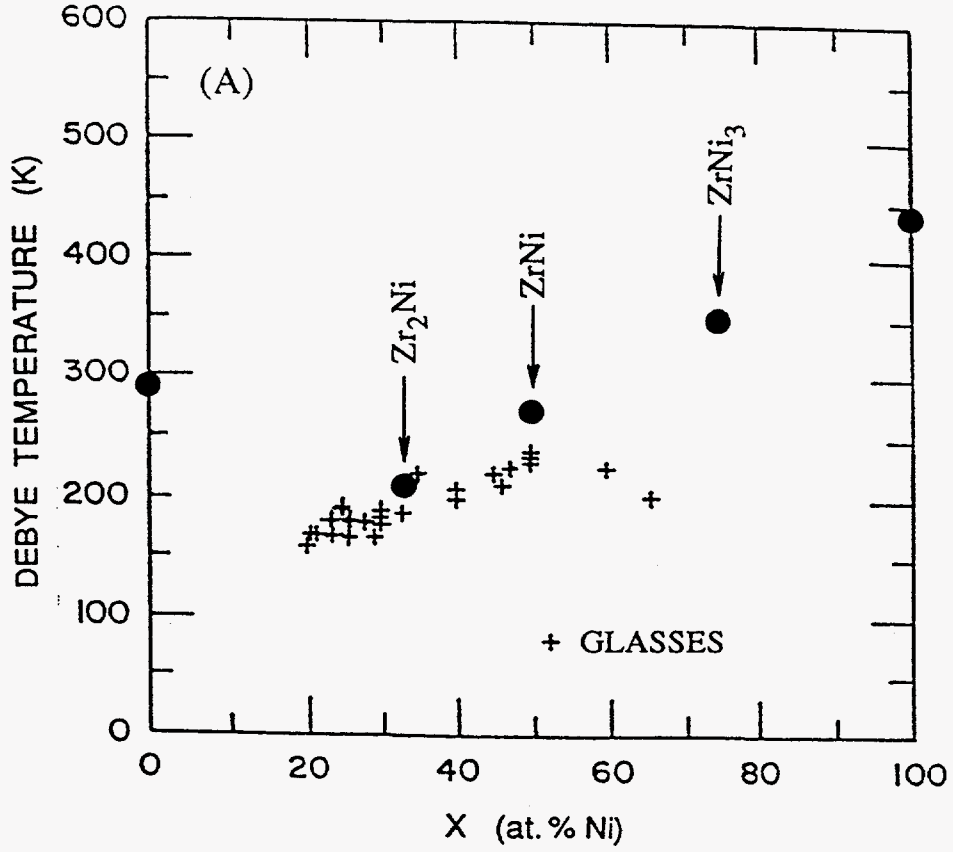
(A)
DEBYE TEMPERATURE (K)
600
500
400
300
200
100
0
0
20
40
60
80
100
X (at.% Ni)
Zr_2Ni
ZrNi
$ZrNi_3$
+ GLASSES

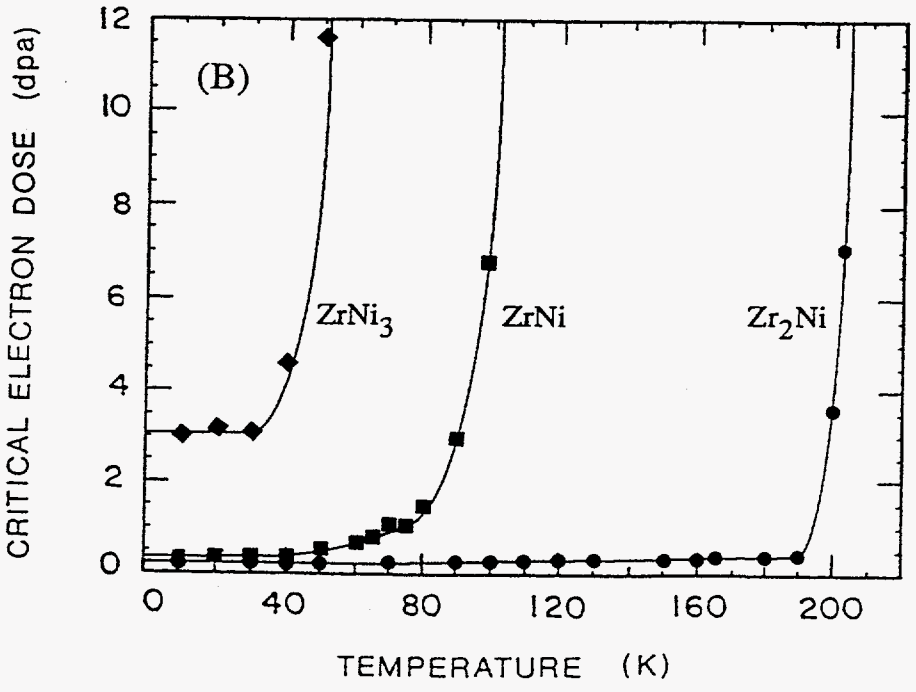
(B)
CRITICAL ELECTRON DOSE (dpa)
12
10
8
6
4
2
0
0
40
80
120
160
200
TEMPERATURE (K)
$ZrNi_3$
ZrNi
Zr_2Ni

Fig. 14

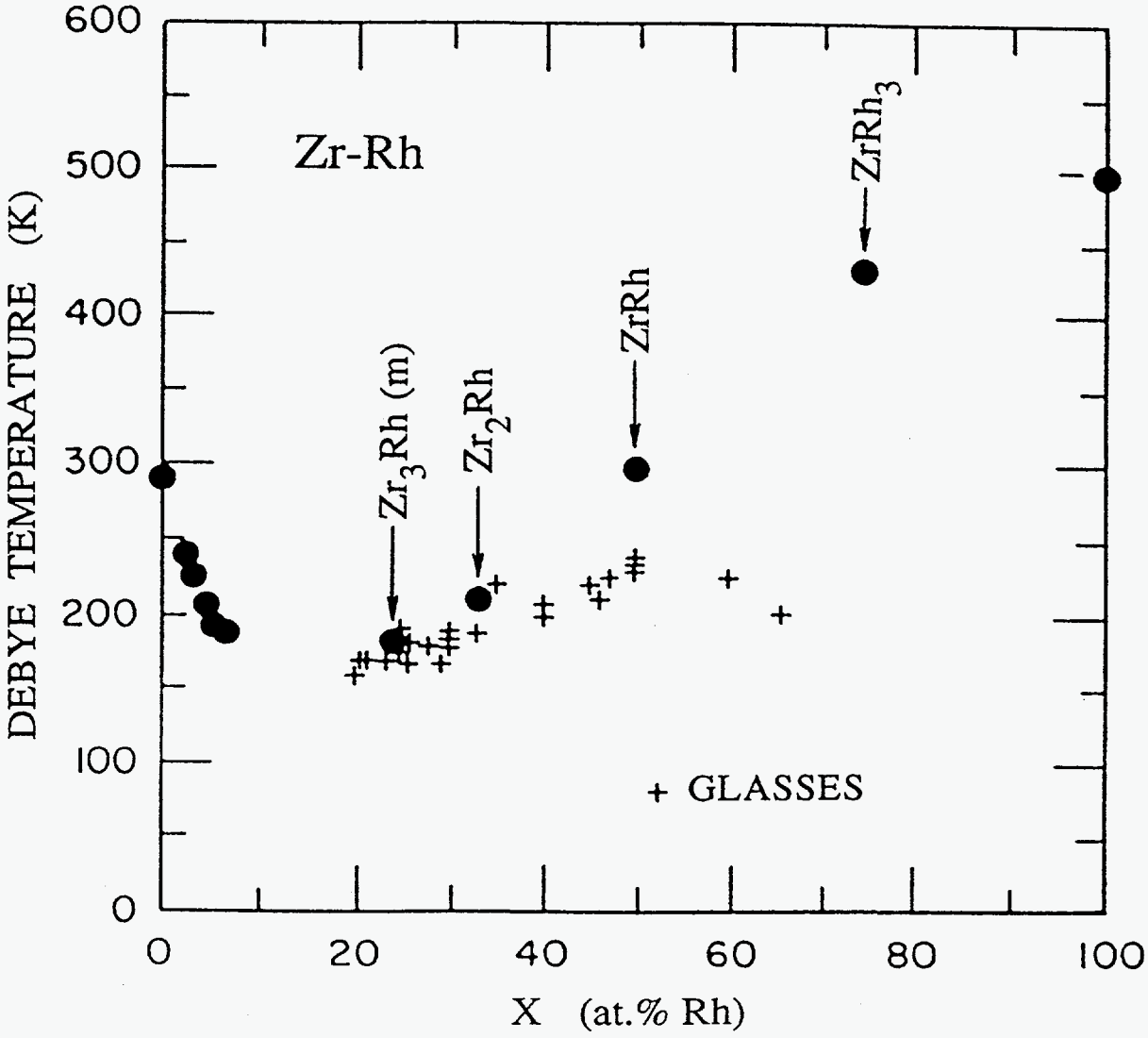
Zr-Rh
DEBYE TEMPERATURE (K)
600
500
400
300
200
100
0
0
20
40
60
80
100
X (at.% Rh)
Zr_3Rh (m)
Zr_2Rh
ZrRh
$ZrRh_3$
+ GLASSES

Fig. 15

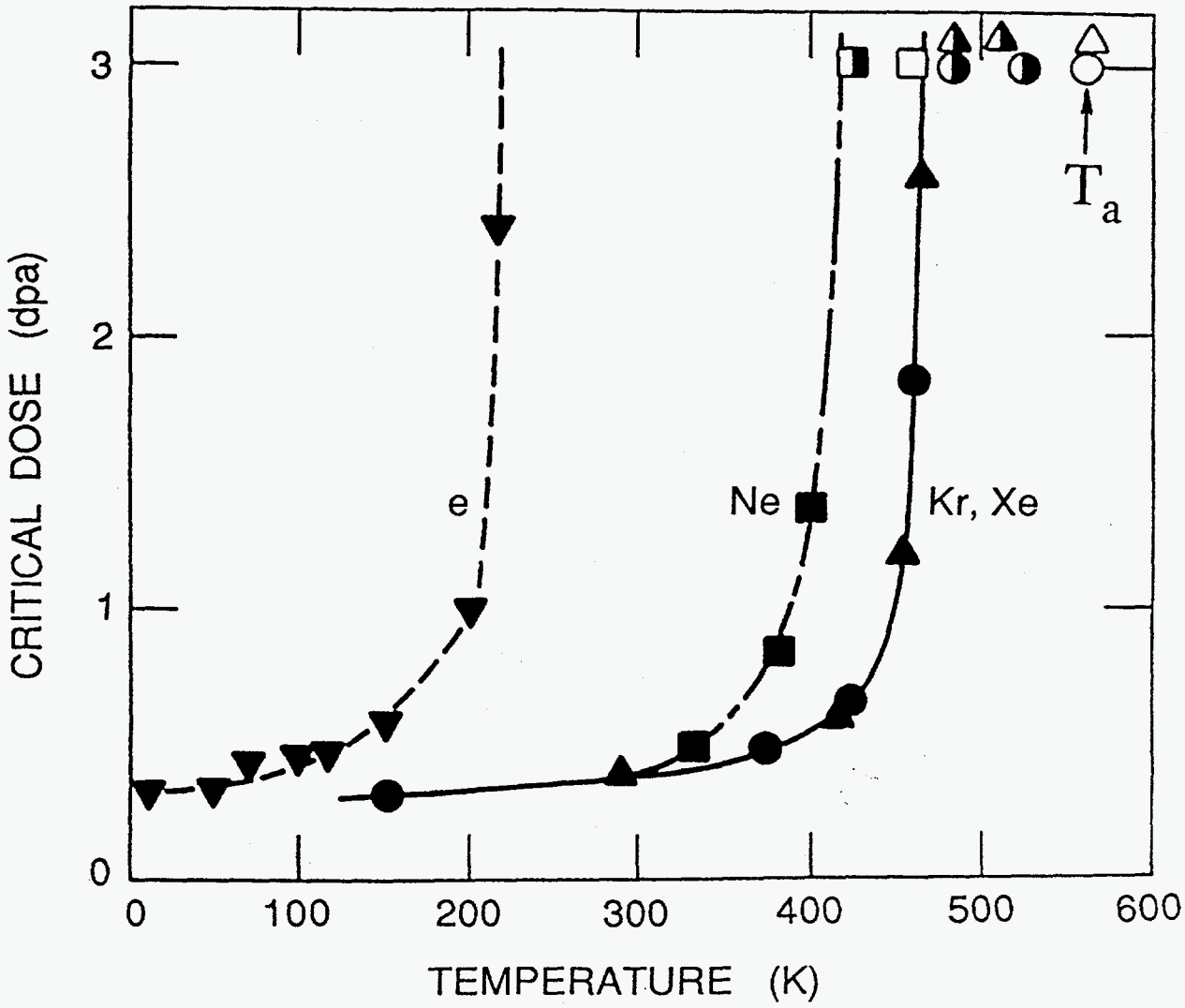
CRITICAL DOSE (dpa)
TEMPERATURE (K)
0
1
2
3
0
100
200
300
400
500
600
e
Ne
Kr, Xe
T_a

Fig. 16